Nanomedicine: Nanotechnology, Biology, and Medicine 57 (2024) 102742

Contents lists available at ScienceDirect

Nanomedicine: Nanotechnology, Biology, and Medicine

journal homepage: www.sciencedirect.com/journal/nanomedicine-nanotechnology-biology-and-medicine

Functionalization and magnetonavigation of T-lymphocytes functionalized via nanocomposite capsules targeting with electromagnetic tweezers

Anatolii Abalymov, PhD [a,c,*], Maxim A. Kurochkin, PhD [a], Sergei German, PhD [a], Aleksei Komlev, MSc [b], Evgeny S. Vavaev, MSc [b], Evgeny V. Lyubin, PhD [b], Andrey A. Fedyanin, DSc (Habilitation) [b], Dmitry Gorin, DSc [a], Marina Novoselova, PhD [a]

[a] Skolkovo Institute of Science and Technology, Moscow 121205, Russia
[b] Lomonosov Moscow State University, Moscow 119991, Russia
[c] Science Medical Center, Saratov State University, 410012 Saratov, Russia

ARTICLE INFO

Keywords:
T-lymphocytes
Layer-by-layer
Freezing-induced loading
Drug delivery systems
Cell delivery

ABSTRACT

Modification of T-lymphocytes, which are capable of paracellular transmigration is a promising trend in modern personalized medicine. However, the delivery of required concentrations of functionalized T-cells to the target tissues remains a problem. We describe a novel method to functionalize T-cells with magnetic nanocapsules and target them with electromagnetic tweezers. T-cells were modified with the following magnetic capsules: Parg/DEX (150 nm), BSA/TA (300 nm), and BSA/TA (500 nm). T-cells were magnetonavigated in a phantom blood vessel capillary in cultural medium and in whole blood. The permeability of tumor tissues to captured T-cells was analyzed by magnetic delivery of modified T-cells to spheroids formed from 4T1 breast cancer cells. The dynamics of T-cell motion under a magnetic field gradient in model environments were analyzed by particle image velocimetry. The magnetic properties of the nanocomposite capsules and magnetic T-cells were measured. The obtained results are promising for biomedical applications in cancer immunotherapy.

Background

According to the World Health Organization (WHO), cancer is the second leading cause of death.[1] Researchers in cancer therapy are confronted with problems with anticancer drugs such as their poor solubility and stability, unwanted toxicity, and/or inability to penetrate cell membranes.[2–4] These problems have led to the development of various drug delivery systems. The rapid progress in nanotechnology has made it possible to incorporate several therapeutic, sensory, and target agents into nanoparticles (liposomes, viruses, quantum dots, etc.) with various size ranges, giving hope for the detection, prevention, and treatment of cancer. The success of these particles depends largely on the choice of suitable design parameters to overcome the physicochemical limitations of free drugs (i.e., solubility and stability) and biological barriers to targeting (i.e., target deposition).[5,6] Polymeric multilayered nano- and microcapsules are promising systems that usually consist of core–shell structures. In these structures, drugs and/or contrast agents can be loaded both in the core and in the shell, which makes it possible to achieve sufficiently high drug loading and to functionalize the surface.[7–18]

Although synthetic drug carriers are being intensely developed for many applications, it is still important to investigate natural particles (both pathogens and mammalian cells), because they have their own delivery mechanisms.[6,8,19] Researchers will attempt to mimic or modify these carriers to deliver various therapeutic payloads that include DNA, vaccines, peptides, and/or proteins and small molecules.[11] Currently, work is underway to use stem cells, mesenchymal cells, phages, and dendritic cells, among others, as such systems.[8,20]

Of particular interest is the functionalization of immune cells with magnetite-containing particles, which makes it possible to combine the target properties of these cells in tissue homing with payloads made of synthetic materials.[21] This approach allows precise localization of modified lymphocytes with particles in the desired area by using a magnetic field gradient,[22] thereby increasing the efficiency of therapy for transferred cells. At present, studies using magnetically guided lymphoid cell delivery to treat cancer and autoimmunity are very limited and this area remains unexplored in detail. However, manipulating highly motile effector lymphoid cells, such as T or natural killer

* Corresponding author at: Skolkovo Institute of Science and Technology, Moscow 121205, Russia.
E-mail address: anatolii.abalymov@gmail.com (A. Abalymov).

https://doi.org/10.1016/j.nano.2024.102742
Received in revised form 7 February 2024;
Available online 7 March 2024

(NK) cells, for targeting and accumulation in areas such as inflamed lymph nodes or solid tumors may be a promising approach to the therapy and visualization of metastases and tumor cells (if a contrast agent is included in the capsule structure).[23,24]

Magnetic targeting of T-lymphocytes revolutionizes immunology with versatile applications. In cancer immunotherapy, it enhances T-cell infiltration into tumor microenvironments, optimizing therapeutic impact while minimizing systemic effects.[25] Adoptive T-cell therapy benefits from improved homing to lymphoid organs, augmenting interactions with antigen-presenting cells for enhanced efficacy.[26] Precision delivery of immunosuppressive agents via magnetic guidance proves effective in autoimmune diseases, concentrating regulatory T-lymphocytes at sites of inflammation.[27] In vaccine development, targeted antigen presentation improves vaccine efficacy by concentrating antigen-presenting T-lymphocytes in lymph nodes.[28] For infectious diseases, magnetic targeting concentrates T-lymphocytes at infection sites and guides them to viral reservoirs for effective clearance. In organ transplantation, graft rejection is potentially reduced through the modulation of immune responses at the graft site. Immunomagnetic imaging allows real-time monitoring of T-cell trafficking, providing valuable insights into the dynamics of immune responses.[29] These applications collectively position magnetic targeting as a powerful tool in immunobiomedical sciences, with ongoing refinements paving the way for translational success.

We hypothesize that lymphocyte cells in a magnetic field can be effectively controlled with polymeric magnetic capsules, which do not penetrate these cells but instead remain on their surface. In addition, we devised a method for making nanoscale magnetic polymer capsules and a system for targeting cells with magnetic tweezers. The aims of this work were to develop new composite materials and a technique for the adsorption of these materials on the T-lymphocyte membrane surface and to develop a technique for magnetic cell targeting by using a magnetic field in a complex medium such as whole blood under flow conditions. To study biological effects, we made detailed cell studies, including analysis of toxicity, cell cumulation, adhesion to the cell surface, and the possibility of capsule transfer from lymphocyte cells to cancerous tumors, represented by cell spheroids.

Methods

Preparation of magnetic nanocomposite capsules (MNCs)

The synthesized $CaCO_3$ particles were used as templates to make MNCs. $CaCO_3$ cores were loaded by the novel freezing-induced loading (FIL) technique,[30] by using a TetraQuant R-1 minirotator (TetraQuant, Russia). In short, 1 mL of $CaCO_3$ particles was mixed with 1 mL of a suspension of magnetic nanoparticles. The mixture was freezed under constant mixing at −20 °C for 2 h. After being thawed, the sample was centrifuged at 8000 rpm for 2 min and was washed three times with DI water. The MNC shell consisted of two bilayers of PARG and DEX or two bilayers of BSA and TA (Fig. 3). Next, the $CaCO_3$ cores were dissolved with 0.2 M EDTA in the case of PARG/DEX MNCs or with 0.1 M HCl in the case of BSA/TA MNCs; this gave rise to polymeric MNCs. After each adsorption step and after the dissolution of the cores, the capsule suspension was purified by centrifugation (8000 rpm, 1 min) and was double washed with 2 mL of DI water. To obtain 150-nm particles, we incubated 300-nm capsules in a thermal shaker at 90 °C for 1 h with constant stirring.

Cell culture

Jurkat cells were cultured in RPMI media supplemented with 10 % fetal bovine serum and penicillin/streptomycin. 4T1 cells were cultured in Dulbecco's modified Eagle's medium (DMEM) supplemented with 10 % fetal bovine serum, penicillin/streptomycin, and 4.5 g/L of glucose. The media for both cultures were replaced every 3 days, and the cells were maintained in a humidified incubator at 5 % CO_2 and 37 °C.

Cell binding to MNCs

Cells (10^6 cells/mL) were placed in a test tube in 1 mL of the culture medium. Capsules were added at 100 MNCs/cell. Then, the tube was put on a rotating panel and placed in an incubator for 2 h. The suspension was centrifuged at 300 rpm for 3 min, and the supernatant liquid was replaced with a fresh culture medium.

Optical setup for lymphocyte imaging

Fig. 1A shows a schematic representation of the experimental setup used for blood cell visualization and for magnetic trapping of functionalized lymphocytes in a phantom capillary. The lymphocytes suspended in the cell medium and those suspended in the whole blood stream were magnetically guided with electromagnetic tweezers, as shown in Fig. 1B and C, respectively.

An optical system for blood cell imaging was constructed on the basis of a self-made inverted microscope that consisted of an M Plan Apo NIR 10×/0.27 microscope objective (Mitutoyo, Japan), a tube lens with a focal length of 200 mm (Thorlabs Inc., Germany), and an acA2040-120um monochrome CMOS image sensor (Basler AG, Germany). Functionalized magnetic lymphocytes were stained with calcein (Sigma–Aldrich) to enable their imaging in the whole blood flow. The fluorescence of the stained lymphocytes was excited with a continuous laser light source (OXlasers, China; 488 nm, 80 mW) and optomechanical components to deliver the laser light through the microscope objective. For this purpose, the laser light was guided coaxially into the optical path of the microscope setup by using two mirrors (M1 and M2) and a long-pass dichroic mirror (D1) with a cut-off wavelength of 500 nm (Fig. 1A). A laser beam with a diameter of 8 mm was focused in the rear focal plane of the objective by using an achromatic doublet with a focal length of 150 mm for the uniform illumination of the sample. Additionally, a dichroic emission filter was placed in front of the microscope tube lens for the fluorescence imaging of lymphocytes. All image sequences were recorded at 114 fps. The exposure time was 5 ms, and the resolution of each micrograph was 2040 × 1536 pixels.

Phantom capillary

The phantom glass capillary had a rectangular cross section with plane-parallel faces to avoid unwanted overreflections on the rounded edges. The capillary had the following dimensions: capillary length, 20 mm; inner channel height, 0.2 mm; inner channel width, 2.68 mm. The capillary was prewashed with heparin and was attached to the edge of the microscope slide with 3D printed clamps.

Magnetic tweezers

These consisted of two electromagnets (Fig. 1A), representing induction coils 70 × 45 mm in size with steel concentrators 120 mm long and 12 mm in diameter, pointed at one end and interconnected at the other with a jumper of the same material to form the southern and northern poles. Each coil consisted of 2000 turns of copper wire with a diameter of 0.5 mm and was powered by an individual laboratory power supply (30 V and 1 A), with opposite polarity for greater efficiency. One of the electromagnets was mounted on the rotary stage to allow precise adjustment of the gap between the two concentrators, the size of which was 2 mm.

The maximum induction of the magnetic tweezers was 0.4 T and the magnetic field gradient G was 1000 G cm^{-1} (Fig. 1D).

$$G = \Delta B/\Delta S, \tag{2}$$

where B is the magnetic flux density and S is the distance.

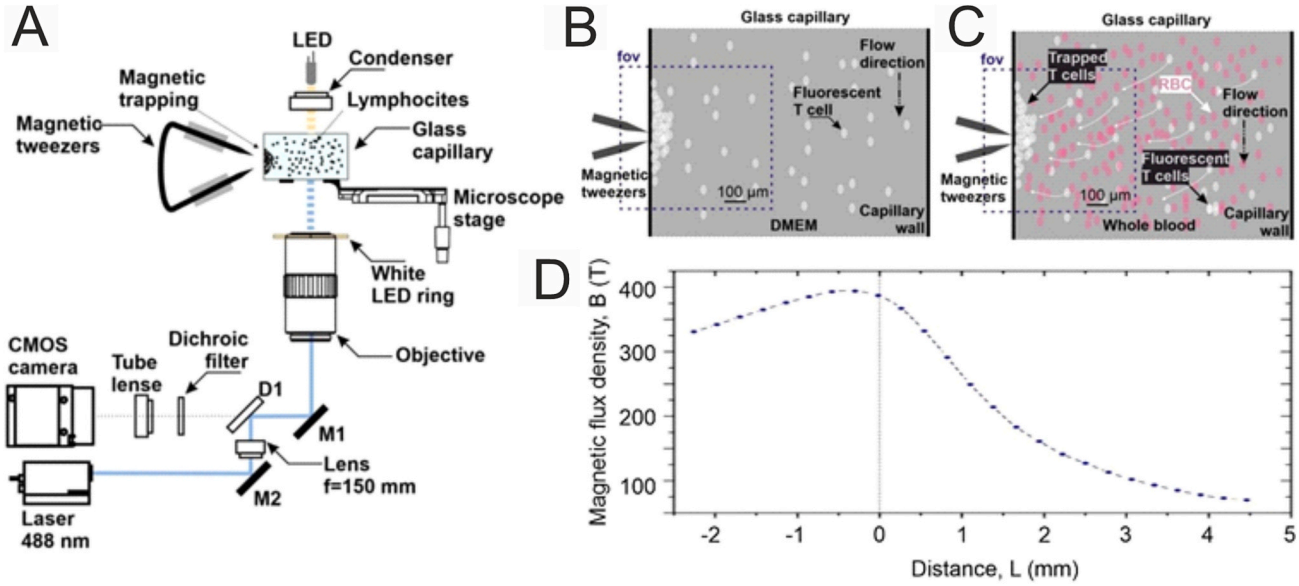

Fig. 1. (A) Experimental setup for imaging and magnetic trapping of functionalized lymphocytes using magnetic tweezers. Schematic representations in (B) depict trapping in DMEM and (C) in whole human blood. The blue dotted line denotes the imaging system's field of view, while white ovals represent lymphocytes and pink ovals denote erythrocytes. (D) presents the B-field versus distance from the magnet tips, with measurements conducted at 22 °C.

Results

The carriers for lymphocyte modification were polymeric MNCs, prepared by layer-by-layer polymer deposition. This technology ensures high loading of both drugs and magnetic nanoparticles for control under the influence of a magnetic field, because it becomes possible to use both core volume and shell capsules.[13,17,18] In addition, the FIL technology, developed by our group, affords even higher loading levels both in the core and in the shell.[30] In search of the optimal size for lymphocyte modification, 150-, 300-, and 500-nm MNCs were prepared. Fig. 2A shows the scheme for MNC preparation.

Nanoparticles of 500 nm were synthesized in a glycerol solution, and those of 300 nm were prepared in an 85 % ethylene glycol solution (Fig. 2A, Step 1). Then, SPIONs were loaded into $CaCO_3$ particles by the FIL method (Fig. 2A, Step 2).[30] The average size of the SPION, as measured by transmission electron microscopy (TEM) and dynamic light scattering (DLS), was 7 ± 2 nm. The iron concentration was 1.06 ± 0.03 mg/mL. The TEM image, size, and z-potential of the SPIONs are shown in Fig. S1. After that, the composite $CaCO_3$/SPION particles were coated with BSA–Cy5/TA (for 500- and 300-nm particles) and PARG–Cy5/DEX (only for 150-nm particles) (Fig. 2A, Step 3). Finally, the dissolution of the $CaCO_3$ cores yielded polymeric magnetic microcapsules of 500 and 300 nm (Fig. 2A, Step 4). The 300-nm capsules were thermally compressed to obtain 150-nm ones (Fig. 2A, Step 5). As shown in Fig. 2A, the PARG/DEX polymers were chosen for 150-nm particles because the BSA/TA capsules degraded when exposed to 90 °C for 1 h.[31]

The results of SEM, DLS, and magnetometer investigations are shown in Fig. 2B–F. The z-potential of the capsules for 150, 300 and 500 nm capsules was −21 ± 1 mV, −17 ± 2 mV, −18 ± 2 mV, respectively.

The MNCs were visualized by SEM (Fig. 2B–D). Fig. 2B shows that the 150-nm MNCs appear denser after thermal shrinkage, which is consistent with our data obtained for 250-nm MNCs made from 500-nm MNCs.[31] The size distribution (150, 300, and 500 nm) obtained by DLS is shown in Fig. 2E. The concentrations of magnetic nanoparticles in the capsules were 0.28, 0.3, and 0.32 pg/capsule for 150-, 300-, and 500-nm MNCs, respectively.

The magnetic properties of the MNCs were evaluated with a magnetometer and optical tweezers. Fig. 2F shows that MNCs of all three sizes have similar magnetic properties, which can be explained as follows. (1) When the particles were loaded by the FIL method, we loaded the same amount of SPIONs into the 500- and 300-nm MNCs. (2) The difference in size between the capsules was relatively small. All hysteresis loops show superparamagnetic behavior, as expected for magnetic nanoparticles of this size. The results obtained with the optical tweezers are presented in Table S1.

We can see that the magnetic moments of the SPIONs are 2.0 ± 0.6, 1.3 ± 0.4, and 2.2 ± 0.3 fA/m^2 for 150, 300 and 500 nm, respectively.

We next developed a protocol for MNC adsorption on the surface of the T-lymphocyte cells (Fig. 3). We used the Jurkat cell culture, which is a widely applied and easy-to-handle model of human T-lymphocytes.[23,32] The most successful adsorption method was to mix $2{\cdot}10^6$ cells with $2{\cdot}10^8$ MNCs in 1 mL of the culture medium for 2 h in a culture incubator. After that, it was important to remove unadsorbed MNCs from the solution. To do this, we used centrifugation at low rotor speed (300 rpm, 3 min). At such low speeds, no MNCs sedimented; yet, the cells sank to the bottom, which enabled us to separate cells with MNCs adsorbed on their surface from unadsorbed MNCs.

The viability of cells in the presence of MNCs was determined by using PrestoBlue fluorescent dye (Fig. 3B–C). Initially, we had to be sure that cell viability was not altered in the presence of MNCs. For this purpose, there was no adsorption of MNCs on the cell surface; instead, MNCs were simply added to the cells in a 96-well plate. The results showed that even at high MNC concentrations (500 MNCs/cell), there was no statistically significant reduction in survival (Fig. 3D).

It was also important to be sure that the adsorption of MNCs on the cell surface and subsequent magnetism did not affect cell survival. To do this, MNCs were adsorbed on T-lymphocytes, as described earlier (Fig. 3A). The test results showed that after magnetization, a slight decrease in cell survival was observed only for MNCs with a size of 150 nm (91 %).

For qualitative assessment of the MNC–lymphocyte interaction, we used confocal fluorescence microscopy. For this purpose, the cells were stained with the intravital dye Calcein Am, which stains the cytoplasm of only living cells. Fig. 3D shows the confocal images of cells for all three sizes of MNCs. As can be seen from Fig. 3D, 150-nm MNCs not only can be located on the membrane surface but also can be taken up by lymphocyte cells, which is confirmed by the orthogonal projection. This effect may explain the slight decrease in survival after magnetization owing to the damage to the cell membrane. Yet, the penetration of 150-nm MNCs into lymphocytes is an interesting fact. It is known from the

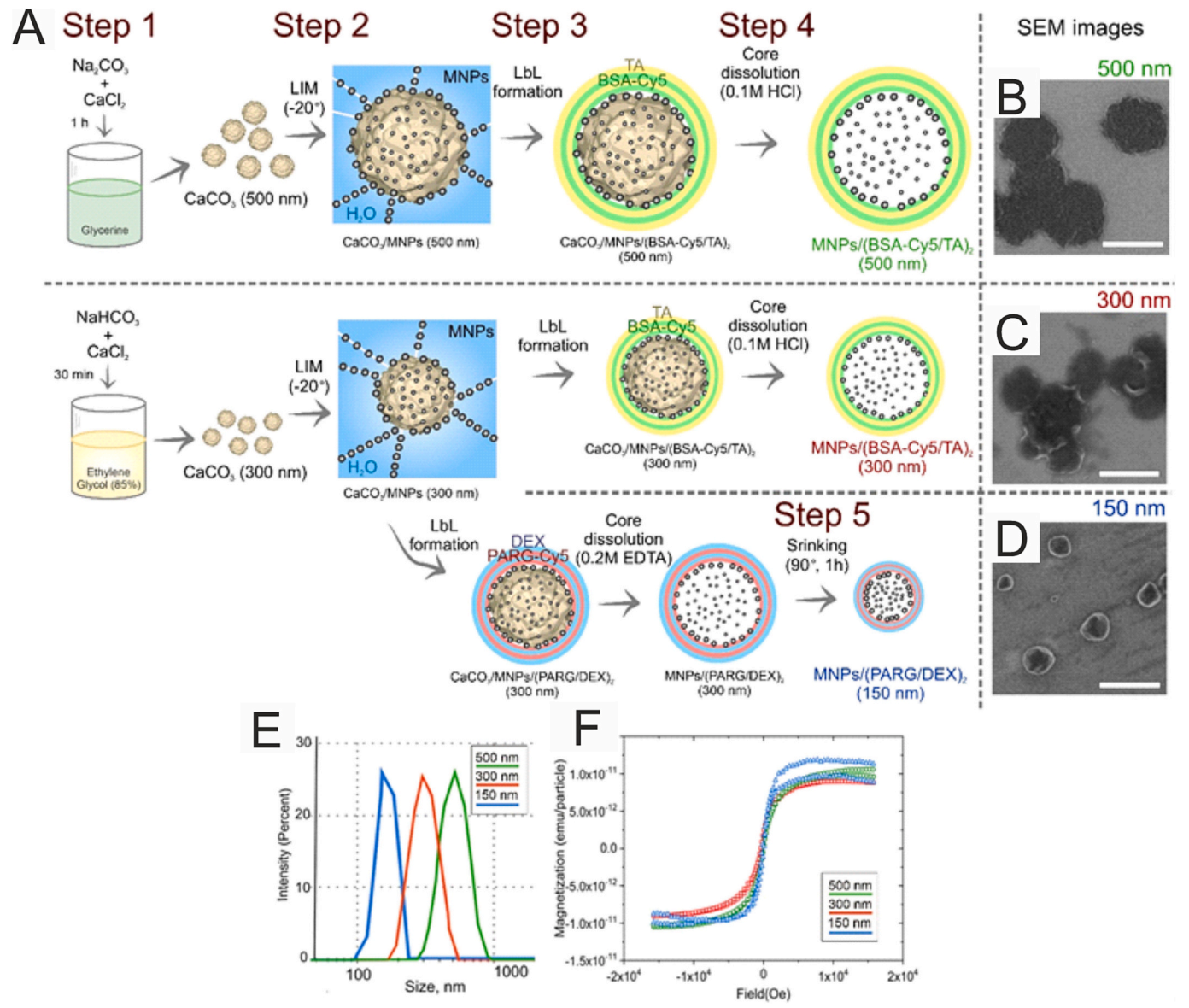

Fig. 2. (A) Schematic representation of MNC preparation. (B–D) SEM images of (B) 150-, (C) 300-, and (D) 500-nm MNCs. Scale bar is 500 nm. (E) Sizes of the MNCs prepared by DLS. (F) Normalized hysteresis loops for water suspensions of various MNCs.

literature that lymphocytes have no phagocytic function, which makes it much more difficult not only for capsules but also for nanoparticles to get inside the cells. Previous experiments have shown that unmodified MNCs accumulate on the cell membrane even after 2 h of coincubation but do not penetrate inside;[33] however, modification of their surface enables them to penetrate the cells.[34,35]

We used two methods to evaluate the adsorption of MNCs on the cell membrane. One was the cumulative probability calculation method. To do this, we used confocal microscopy images (Figs. 4A, S2A). The cumulative probability graph shows that MNCs with a size of 300 nm absorbed the best on the cell surface (Figs. 4B, S2B). MNCs with a size of 150 nm absorbed the worst, and 10 % of the cells from the total number did not have particles on their surface, which may indicate a poor linkage between the T-lymphocyte membrane and dextran sulfate (the last layer of the 150-nm MNCs). These data confirm the results of flow cytometry (Fig. 4C–F). The plot with the 150-nm particles shows a large cloud of points that are free particles (18.21 % ~ 3642 MNCs for $2{\cdot}10^5$ events) (Fig. 4D). MNCs of 300 nm bound to the capsules better (94.08 % of the objects that have double fluorescence) (Fig. 4E). On the basis of the data from magnetometry, flow cytometry, and fluorescence microscopy, we conclude that 300-nm MNCs are the most promising, because they best connect to the surface of the lymphocytes and their magnetic properties do not statistically differ from those of other capsules. It is also important to note that 300-nm capsules do not penetrate inside the cells, which does not violate the integrity of their membranes and does not affect their properties.

When a magnetic field is used in lymphocyte control, it is important to know that magnetization of cells is possible in a flow whose velocity corresponds to that of the fluid flow in in vivo systems. The system can be called successful if we can control the motion of cells in the flow and keep them at the desired sites with a magnetic field both in the cellular environment and in whole blood. This makes the task much more difficult, because in the presence of blood form elements in the flow, the sail effect may complicate the magnetization of cells in the moving fluid. For this purpose, we developed a system consisting of a capillary and a syringe pump that enabled the motion of not only cell medium but also whole blood.

After that, we used the previously described system (Fig. 1A) to see whether it was possible to capture the modified lymphocytes in a magnetic field. Lymphocytes moved along the capillary in a flow of the

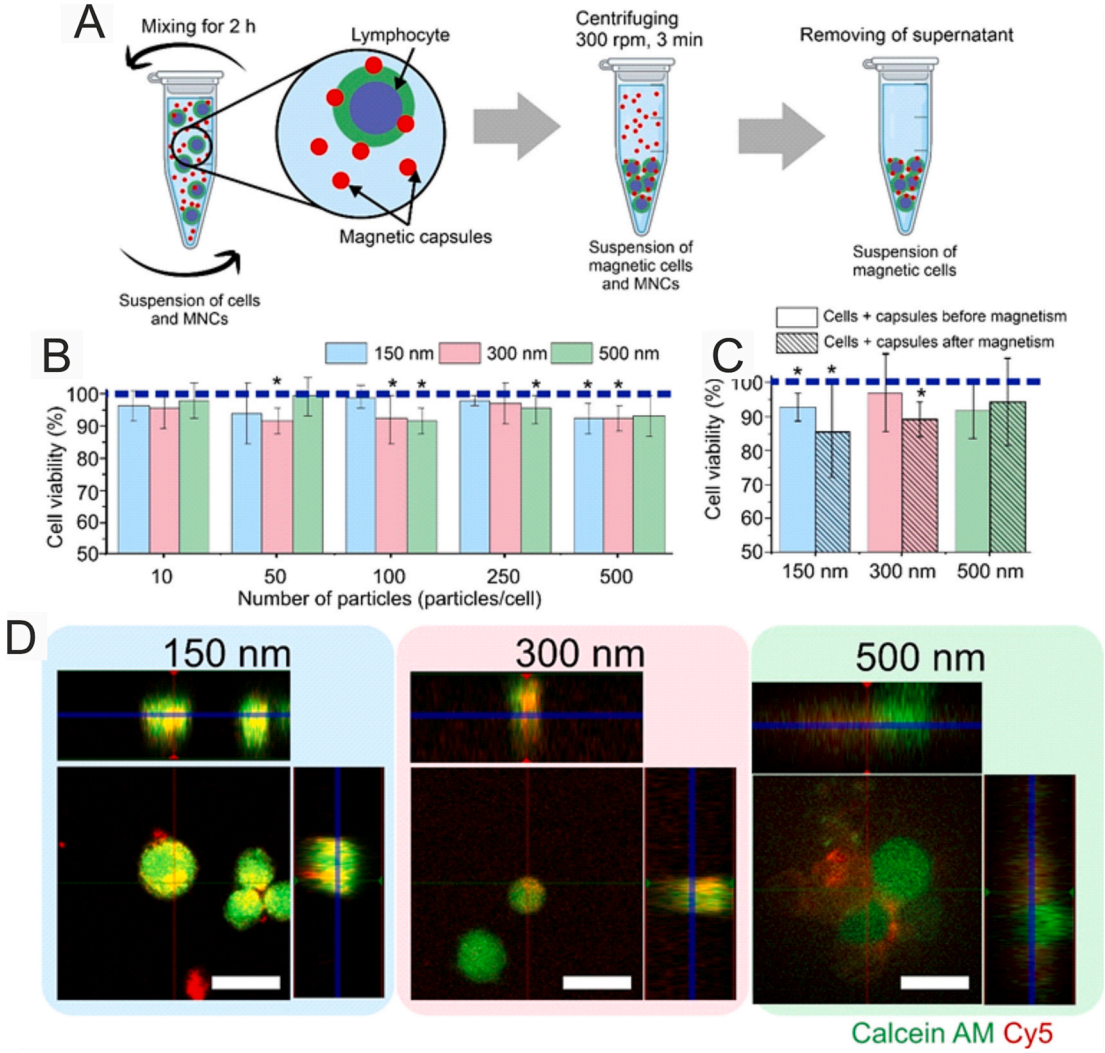

Fig. 3. (A) Scheme for the loading of T-lymphocytes with MNCs. (B–C) Results of experiments on lymphocyte survival during (B) co-incubation with particles and (C) after binding of cells to MNCs. (D) Confocal images of cells, with MNCs present on the cell membrane and into the cells.

culture medium (Fig. 5A, C and E). After the beginning of the motion, magnetic tweezers were switched on, which attracted the cells to the capillary wall through the magnetic field (Fig. 5B, D and F). As seen from the figure, after 10 min of magnetization, the results are very different. In the case of 150-nm MNCs, the cells have very weak magnetization and are practically not entrapped by the magnetic tweezers (Fig. 5B). In the case of 300- and 500-nm MNCs, one can observe the formation of cell colonies on the capillary surface, which indicates that the cells can be captured. However, the number of cells modified by the 300-nm capsules on the surface of the capillary is much higher, indicating the possibility of capturing cells not only at the walls of the capillary but also from the center, where the flow speed is higher (Fig. 5B). Then, to simulate the magnetic trapping of the cells in blood vessels, we used 300-nm MNCs, which performed the best in our preliminary experiments.

At first, the functionalized lymphocytes were resuspended in DMEM and were pumped through this capillary (Fig. 6A–D). In all experiments, the flow rate of the liquid pumped through the capillary was 1 mm/s. After that, sequential microphotographs of the motion of functionalized lymphocytes through the model capillary without magnetic field activation were recorded for 5 min. Then, the magnetic tweezers were activated and the lymphocytes were magnetically captured for 10 min.

As shown in Fig. 6B, after activation of the magnetic tweezers, a zone with trapped lymphocytes was formed in the near-wall area of the capillary, where the tweezer tips were located. The lymphocytes were captured from the flow through their motion along the magnetic field gradient toward the tweezer tips. PIV analysis (Fig. 6C) indicated that cell flow motion before tweezer activation was uniform, straightforward, and parallel to the capillary wall. After the magnetic tweezers had been activated, the direction of lymphocyte motion changed from that straight along the DMEM flow to that toward the tweezers, including against the flow direction (Fig. 6D). Because the rate of motion of functionalized lymphocytes under a magnetic field was, on average, two times higher than the rate of blood flow through the capillary and because the lymphocytes in the flow were unevenly distributed owing to the effect of the magnetic gradient, there were cell-free zones in the optical system's field of view, corresponding to the low-velocity areas on the PIV map. Similar effects have also been described in our previous work.[36]

For evaluating the possibility of capturing modified lymphocytes from the blood stream while they move through the blood or lymphatic vessels, functionalized lymphocytes were dispersed in whole blood and then pumped through the phantom capillary (Fig. 6E–L). The bright-field microscopy images of the flow of functionalized lymphocytes mixed with whole blood are presented in Fig. 6E–H. As can be seen, it was difficult to detect targeted cells in whole blood, but the magnetic motion of the lymphocytes created enough brightness fluctuations, so it was possible to visualize changes in the direction of lymphocyte motion

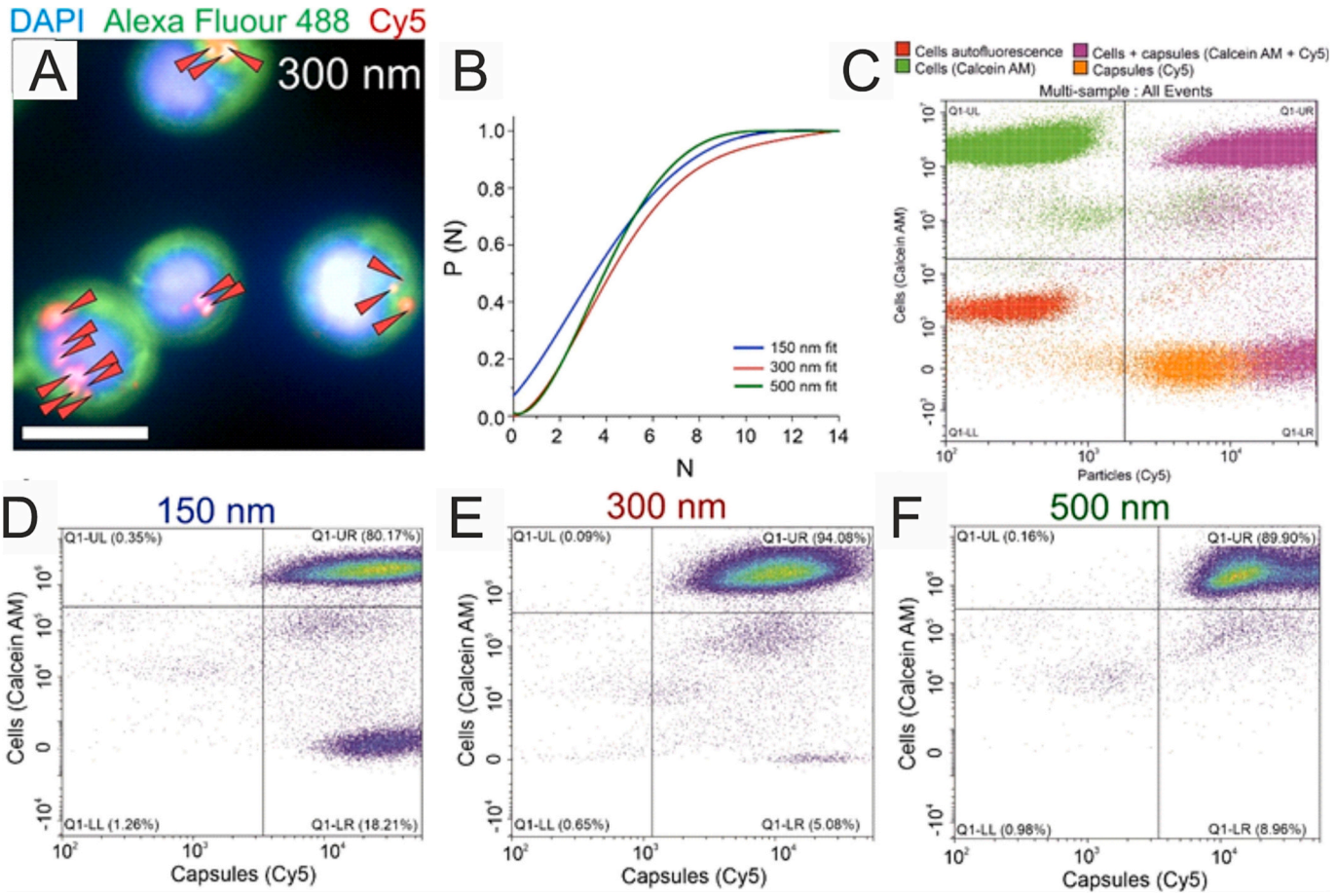

Fig. 4. (A) Confocal images of T-lymphocyte cells with MNCs. Arrows point to MNCs on the cell surface. (B) Fitting of the cumulative probability curves. (C) Example of cytometry results for the detection of MNCs on the T-cells surface. (D–F) Flow cytometry after absorbance of (D) 150-, (E) 300-, and (F) 500-nm MNCs on the cell membrane.

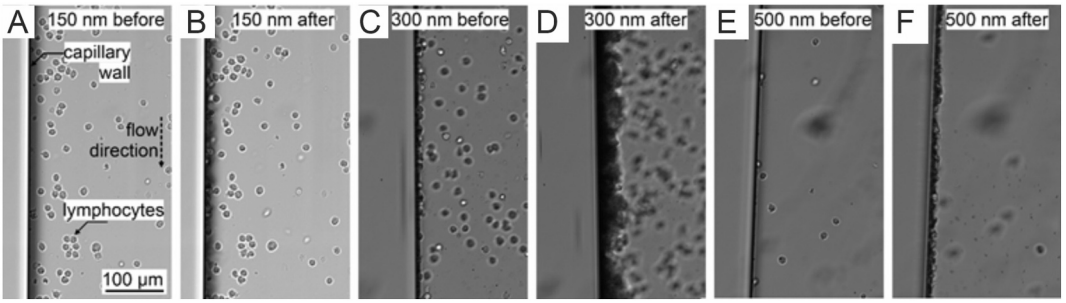

Fig. 5. Magnetic capture of lymphocytes functionalized with (A–B) 150-, (C–D) 300-, and (E–F) 500-nm MNCs in a DMEM flow before and after 10 min of magnetization by electromagnetic tweezers.

through PIV analysis (Fig. 6G–H).

We next analyzed the fluorescence images of calcein-stained lymphocytes in the whole blood flow before (Fig. 6I) and after (Fig. 6J) tweezer activation. Because functionalized lymphocytes are not evenly distributed in whole blood, the velocity vectors on the PIV maps will not be evenly distributed in their values. In Fig. 6J, L, the area of captured lymphocytes is marked in gray with an overlay of transparency. The fluorescence in this region is less owing to the high cell density in this region along with the large number of iron oxide particles, which quench cell fluorescence.

Three-dimensional cell systems (e.g., organoids and spheroids) can be excellent models for tumors in vitro.[37,38] Such models make it possible to ensure that with a magnetic field, we can provide contact between tumor cells and particles in the case of cell-mediated delivery of molecules———that is, to ensure that T-cells contact tumor cells, if we consider this system as a magnetic-mediated cell therapy. For this purpose, we formed spheroids from 4T1 cells, which are breast cancer cells and represent an in vitro tumor model.

Fig. 7A shows the design of an experiment on the magnetic delivery of T-cells functionalized with submicron-sized MNCs to target cell spheroids, with subsequent transfer of these MNCs from the T-cells to the target cell spheroids. A hole with a diameter of 4 mm was formed in a plastic cuvette in one of the measuring sides at a distance of 1.5 mm from the open end. After that, 1 mL of DMEM was added to the cuvette and two cell spheroids were placed in one of the two corners at the base of the cuvette opposite to the corners adjacent to the side of the cuvette

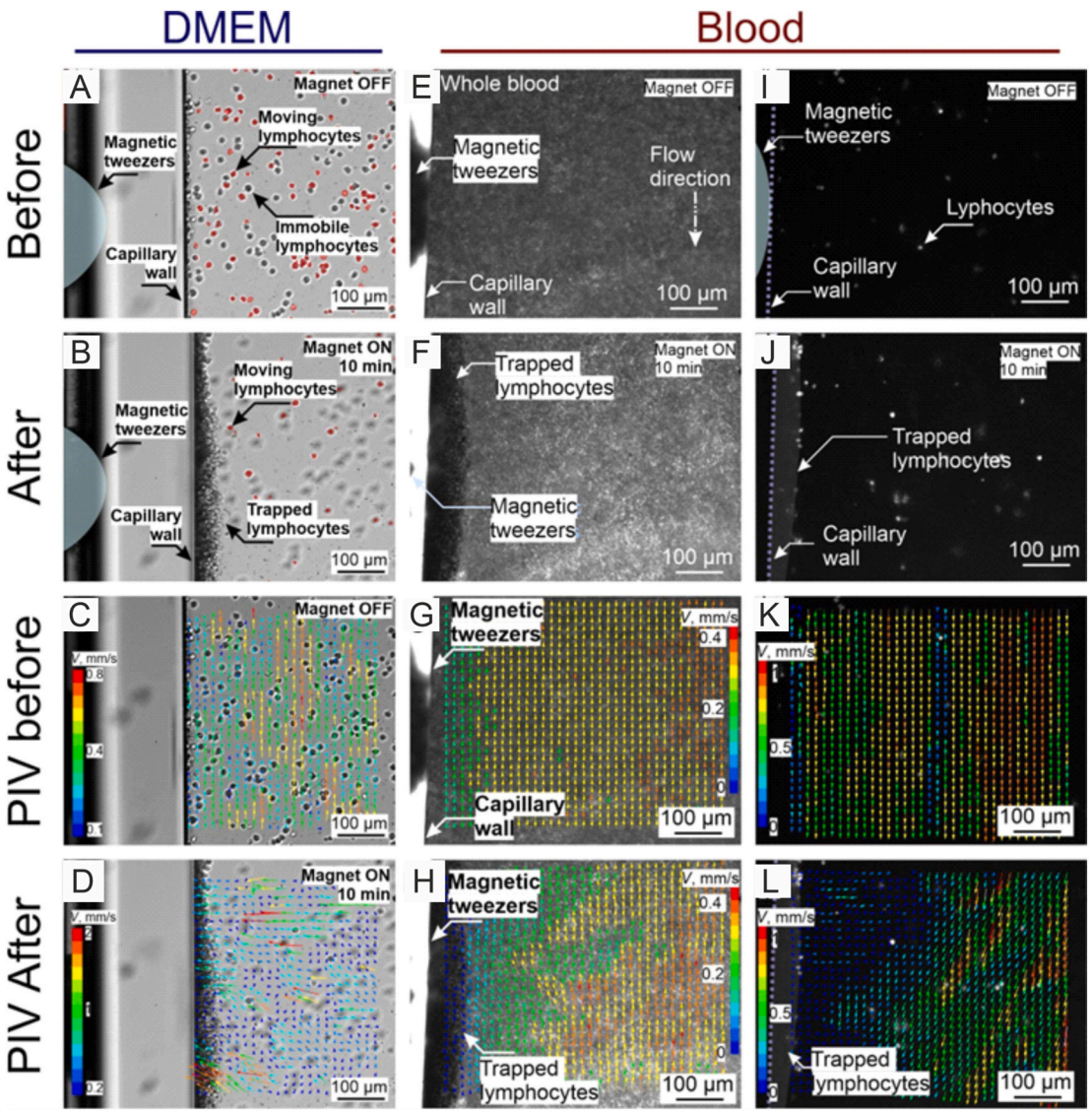

Fig. 6. Magnetic capture of functionalized lymphocytes in both DMEM and whole blood flows using electromagnetic tweezers. Panels (A–D) show bright-field microscopy images and particle image velocimetry (PIV) maps of lymphocytes in DMEM flow (A, C) before and (B, D) after tweezer activation. (E–H) Images and maps for lymphocytes magnetonavigation in whole blood flow (E, G) before and (F, H) after tweezer activation. (I–L) Additional fluorescence microscopy images in panels highlighting magnetoresponsive lymphocytes (I, K) before and (J, L) after tweezer activation.

with the formed hole. The cuvette was closed with the cap and fixed on the microscope stage with the hole upward. Then, magnetic tweezers were placed in the area where the spheroids were located at a distance of 2 mm from them.

After that, 100 μL of a suspension of T-cells functionalized with 10^6 cells/mL of MNCs was added through the formed hole in the cuvette by using a micropipette. The magnetic field of the electromagnetic tweezers was activated, and the motion of T-cells with MNCs toward the spheroid was recorded with 114 fps. The T-cells with MNCs in the area of the cuvette with cellular spheroids were magnetically localized for 5 min. The dynamics of the T-cells under a gradient magnetic field were visualized on a handmade inverted transmitted light microscope with a Zeiss A-Plan 5×/0.12 objective, as shown in Fig. 7A. The bright-field image of a cell spheroid with magnetically attracted T-cells with 300 nm MNCs is presented in Fig. 7B. The two large black spherical objects in the left half of the frame are a pair of cell spheroids, and the smaller spherical patterns shown in Fig. 7B are T-cells, whose color [black (out of focus) or white (in focus)] depends on their localization relative to the objective's focal plane.

Fig. 7C shows the velocity distribution field of the MNC-functionalized T-cells under the effect of the magnetic field. T-cell velocities were measured through PIV analysis in 1000 consecutive frames. The size of the interrogation regions of PIV analysis was 30 × 30 pix each. The velocity map of the T-cells shows that their motion was ordered along the magnetic field gradient in the direction of the magnetic tweezers' location.

We used fluorescence and confocal microscopy to study spheroids after remagnetization of T-lymphocytes. A cuvette with spheroids and magnetic T-lymphocytes was transferred to an Operetta CLS confocal microscope. At this step, we visualized capsules on the spheroid surface. Fig. 7D clearly shows a large accumulation of MNCs (Cy5, red fluorescence) at the periphery of the spheroid, confirming the successful remagnetization of the T-lymphocytes. Fig. 7E, F shows that the presence of lymphocytes on the surface is mediated precisely by remagnetization with MNCs. In the analyzed segment of the spheroid section in Fig. 7F, we can see how the MNCs are distributed as a layer on the surface of the T-cells. After the T-cells are localized on the cell spheroid, some MNCs are transferred to the surface of this spheroid, which is represented as areas of red fluorescence of MNCs Cy5 between the green fluorescence of the T-cells and the blue fluorescence of the spheroid in

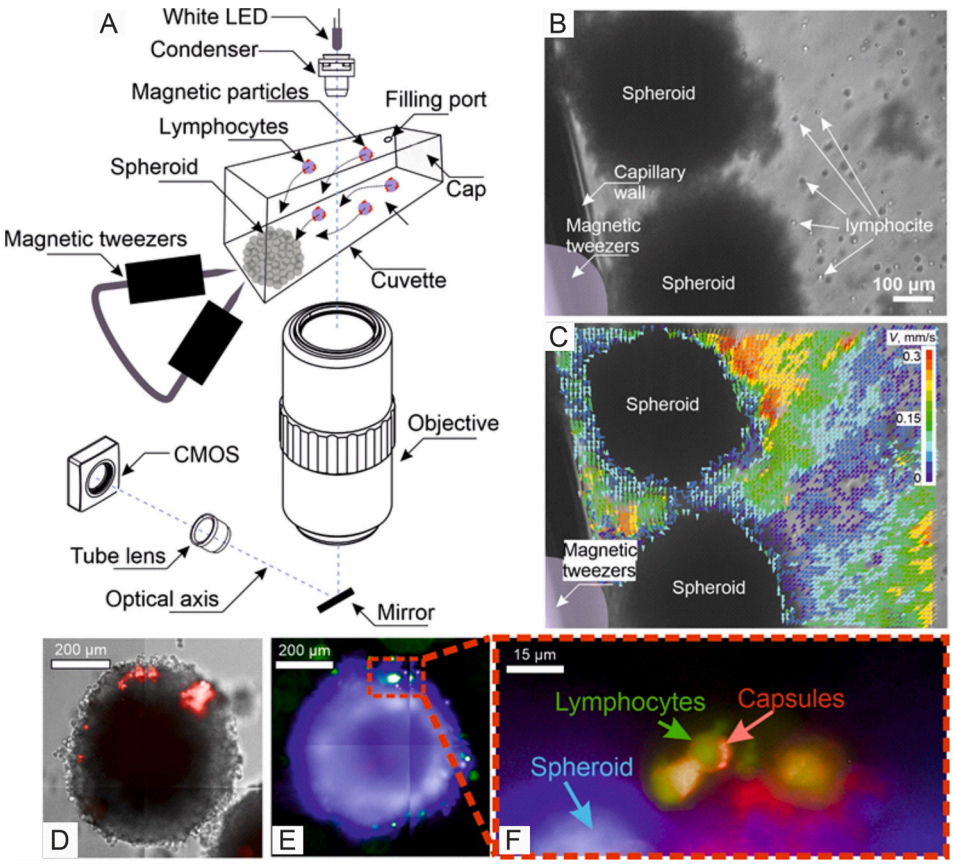

Fig. 7. Demonstration the magnetically controlled incorporation of functionalized T-cells into cell spheroids using magnetic tweezers. (A) Scheme of experimental setup for in vitro magnetic delivery of T-cells to targeted spheroids in a phantom channel. (B) displays a bright-field image of spheroids in a T-cell flow. (C) Particle image velocimetry (PIV) visualization of magnetically affected T-cells in the magnetic field gradient. (D) depicts overlap of bright-field and fluorescence microscopy of a 4T1 spheroid and 300-nm fluorescent MNCs. (E–F) Fluorescence microscopy images of a 4T1 spheroid with delivered T-cells.

the right part of Fig. 7F. This confirms the transfer of 300-nm MNCs from the surface of the T-cells to the cell spheroid through the action of the magnetic field gradient.

Discussion

The presented study on MNCs for lymphocyte modification and magnetic manipulation encapsulates a significant stride in the realm of nanomedicine. The meticulous exploration of three MNC sizes reflects a strategic approach, aligning with the ongoing pursuit of optimal dimensions for nanocarrier efficiency. This sizing strategy finds resonance in existing literature where tailored nanocarriers have demonstrated superior cellular interactions.[39,40]

The observed biocompatibility of T-lymphocytes in the presence of MNCs, even at heightened concentrations, reinforces the promise of these nanocarriers for maintaining cell integrity—a pivotal requirement in biomedical applications.[41,42] The intriguing capability of 150-nm MNCs to penetrate lymphocytes introduces a novel facet, positioning these nanocarriers as potential intracellular delivery agents. This unique feature diverges from traditional carriers, pointing toward emerging trends in intracellular drug delivery strategies.[43,44] Comparatively, the superior binding efficiency of 300-nm MNCs to T-lymphocyte membranes underscores the critical importance of surface interactions in cellular targeting. This finding aligns with existing literature, emphasizing the nuanced influence of nanocarrier characteristics on surface binding and subsequent cellular responses.[45]

The successful simulation of lymphocyte magnetization in a dynamic flow system, particularly the adept manipulation observed with 300-nm MNCs, brings these nanocarriers into the forefront of applications in dynamic biological environments. This controlled motion holds promise for addressing challenges posed by physiological flows—an essential consideration for in vivo applications.[46,47] Drawing on comparative insights, the capability of 150-nm MNCs to penetrate lymphocytes and the superior surface binding efficiency of 300-nm MNCs highlight the versatility and tunability of these nanocarriers for specific applications. This aligns with the evolving landscape of nanomedicine where tailoring nanocarriers to specific cell types and physiological conditions is pivotal for translational success.[48,49]

Looking ahead, the observed efficacy in simulated flow systems provides a springboard for in vivo applications. Future studies could delve into the behavior of MNC-functionalized lymphocytes in complex biological milieus, addressing challenges posed by blood flow and dynamic cellular environments. The optimization of MNC size and surface modifications emerges as a critical avenue for advancing these nanocarriers toward clinical translation. In conclusion, the discussion elucidates the multifaceted potential of polymeric MNCs, emphasizing their role in targeted drug delivery, magnetic manipulation of immune cells, and the evolving landscape of nanomedicine. The results pave the way for future investigations, contributing to the continuous refinement of nanocarrier design and application in biomedical contexts.

In summary, an advanced drug delivery system centered on T-cells modified with magnetic nanocapsules was developed, showcasing their maneuverability using electromagnetic tweezers within controlled environments. The investigation involved a thorough examination of capsules ranging from 150 to 500 nm in size, with the aim of identifying the optimal configuration for lymphocyte modification. Among these sizes, 300-nm MNCs emerged as the ideal candidates for efficient modification and transfer of lymphocytes. Functionalized lymphocytes

were successfully magnetically captured in simulated blood flow scenarios, illustrating their potential as versatile drug carriers, particularly in targeted cancer therapy applications.

CRediT authorship contribution statement

Anatolii Abalymov: Writing – review & editing, Writing – original draft, Visualization, Methodology, Investigation, Formal analysis, Conceptualization. **Maxim A. Kurochkin:** Writing – original draft, Visualization, Methodology, Investigation, Formal analysis. **Sergei German:** Writing – review & editing, Methodology, Investigation, Formal analysis. **Aleksei Komlev:** Writing – review & editing, Investigation, Formal analysis. **Evgeny S. Vavaev:** Writing – review & editing, Methodology, Investigation, Formal analysis. **Evgeny V. Lyubin:** Writing – review & editing, Methodology, Investigation. **Andrey A. Fedyanin:** Supervision, Formal analysis. **Dmitry Gorin:** Writing – review & editing, Supervision, Conceptualization. **Marina Novoselova:** Writing – review & editing, Writing – original draft, Supervision, Resources, Project administration, Methodology, Investigation, Formal analysis, Conceptualization.

Declaration of competing interest

The authors report no conflict of interest in this work.

Acknowledgments

This work was supported by RSCF project N№ 20-74-10114. The visualization and evaluation of the magnetic capture of functionalized lymphocytes using magnetic tweezers were supported by RFBR grant No. 19-32-60058. The obtaining a 4T1 spheroid and a study on the internalization of particles into a spheroid were supported the Grants Council for junior postdoc in Russian Federation (MK-933.2022.3). Zeta-potential, DLS, CLSM and fluorescent microscopy were performed using the equipment of the "Bioimaging and Spectroscopy" Core Facility of the Skolkovo Institute of Science and Technology.

Appendix A. Supplementary data

Supplementary data to this article can be found online at https://doi.org/10.1016/j.nano.2024.102742.

References

1. Bray F, Ferlay J, Soerjomataram I, Siegel RL, Torre LA, Jemal A. Global cancer statistics 2018: GLOBOCAN estimates of incidence and mortality worldwide for 36 cancers in 185 countries. *CA Cancer J Clin*. 2018;68(6):394–424.
2. Cheng Z, Li M, Dey R, Chen Y. Nanomaterials for cancer therapy: current progress and perspectives. *J Hematol Oncol*. 2021;14(1):1–27.
3. Narvekar M, Xue HY, Eoh JY, Wong HL. Nanocarrier for poorly water-soluble anticancer drugs - barriers of translation and solutions. *AAPS PharmSciTech*. 2014;15(4):822–833.
4. Mitchell MJ, Billingsley MM, Haley RM, Wechsler ME, Peppas NA, Langer R. Engineering precision nanoparticles for drug delivery. *Nat Rev Drug Discov*. 2021;20(2):101–124.
5. Danaei M, Dehghankhold M, Ataei S, et al. Impact of particle size and polydispersity index on the clinical applications of lipidic nanocarrier systems. *Pharmaceutics*. 2018;10(2):1–17.
6. Finbloom JA, Sousa F, Stevens MM, Desai TA. Engineering the drug carrier biointerface to overcome biological barriers to drug delivery. *Adv Drug Deliv Rev*. 2020;167:89–108.
7. Galogahi FM, Zhu Y, An H, Nguyen NT. Core-shell microparticles: generation approaches and applications. *J Sci Adv Mater Devices*. 2020;5(4):417–435.
8. Yoo JW, Irvine DJ, Discher DE, Mitragotri S. Bio-inspired, bioengineered and biomimetic drug delivery carriers. *Nat Rev Drug Discov*. 2011;10(7):521–535.
9. Volodkin DV, Petrov AI, Prevot M, Sukhorukov GB. Matrix polyelectrolyte microcapsules: new system for macromolecule encapsulation. *Langmuir*. 2004;20(8):3398–3406.
10. Abalymov AA, Verkhovskii RA, Novoselova MV, et al. Live-cell imaging by confocal Raman and fluorescence microscopy recognizes the crystal structure of calcium carbonate particles in HeLa cells. *Biotechnol J*. 2018;13(11), 1800071.
11. Morachis JM, Mahmoud EA, Almutairi A. Physical and chemical strategies for therapeutic delivery by using polymeric nanoparticles. *Pharmacol Rev*. 2012;64(3):505–519.
12. Szafraniec-Szczęsny J, Janik-Hazuka M, Odrobińska J, Zapotoczny S. Polymer capsules with hydrophobic liquid cores as functional nanocarriers. *Polymers (Basel)*. 2020;12(9):1–25.
13. Mokrousov MD, Thompson W, Ermilov SA, et al. Indocyanine green dye based bimodal contrast agent tested by photoacoustic/fluorescence tomography setup. *Biomed Opt Express*. 2021;12(6):3181.
14. Novoselova MV, Bratashov DN, Sarimollaoglu M, et al. Photoacoustic and fluorescent effects in multilayer plasmon-dye interfaces. *J Biophotonics*. 2019;12(4).
15. Novoselova MV, Voronin DV, Abakumova TO, et al. Focused ultrasound-mediated fluorescence of composite microcapsules loaded with magnetite nanoparticles: in vitro and in vivo study. *Colloids Surf B Biointerfaces*. 2019;181:680–687.
16. Novoselova MV, German SV, Sindeeva OA, et al. Submicron-sized nanocomposite magnetic-sensitive carriers: controllable organ distribution and biological effects. *Polymers (Basel)*. 2019;11(6):1–23.
17. Novoselova MV, Shramova EI, Sergeeva OV, et al. Polymer/magnetite carriers functionalized by HER2-DARPin: avoiding lysosomes during internalization and controlled toxicity of doxorubicin by focused ultrasound induced release. *Nanomed Nanotechnol Biol Med*. 2023;47, 102612.
18. Novoselova MV, German SV, Abakumova TO, et al. Multifunctional nanostructured drug delivery carriers for cancer therapy: multimodal imaging and ultrasound-induced drug release. *Colloids Surf B Biointerfaces*. 2021;200(December 2020).
19. Anselmo AC, Mitragotri S. Cell-mediated delivery of nanoparticles: taking advantage of circulatory cells to target nanoparticles. *J Control Release*. 2014;190:531–541.
20. Studeny M, Marini FC, Dembinski JL, et al. Mesenchymal stem cells: potential precursors for tumor stroma and targeted-delivery vehicles for anticancer agents. *J Natl Cancer Inst*. 2004;96(21):1593–1603.
21. Lian SWM, Guo S, Ren K, Xu Y, Ho JS, Chen CH. Heterogeneous multi-compartmental DNA hydrogel particles prepared: via microfluidic assembly for lymphocyte-inspired precision medicine. *Nanoscale*. 2021;13(48):20531–20540.
22. Swiston AJ, Cheng C, Um SH, Irvine DJ, Cohen RE, Rubner MF. Surface functionalization of living cells with multilayer patches. *Nano Lett*. 2008;8(12):4446–4453.
23. Steinfeld U, Pauli C, Kaltz N, Bergemann C, Lee HH. T lymphocytes as potential therapeutic drug carrier for cancer treatment. *Int J Pharm*. 2006;311(1–2):229–236.
24. Mühlberger M, Janko C, Unterweger H, et al. Functionalization of T lymphocytes with citrate-coated superparamagnetic iron oxide nanoparticles for magnetically controlled immune therapy. *Int J Nanomedicine*. 2019;14:8421–8432.
25. Tang H, Wang Y, Chlewicki LK, et al. Facilitating T cell infiltration in tumor microenvironment overcomes resistance to PD-L1 blockade. *Cancer Cell*. 2016;29(3):285–296.
26. Yang JC, Rosenberg SA. Adoptive T-cell therapy for cancer. In: *Advances in Immunology*. vol. 130. 2016:279–294.
27. Barnett BP, Arepally A, Karmarkar PV, et al. Magnetic resonance-guided, real-time targeted delivery and imaging of magnetocapsules immunoprotecting pancreatic islet cells. *Nat Med*. 2007;13(8):986–991.
28. Angel CE, Chen CJJ, Horlacher OC, et al. Distinctive localization of antigen-presenting cells in human lymph nodes. *Blood*. 2009;113(6):1257–1267.
29. Mehling M, Frank T, Albayrak C, Tay S. Real-time tracking, retrieval and gene expression analysis of migrating human T cells. *Lab Chip*. 2015;15(5):1276–1283.
30. German SV, Novoselova MV, Bratashov DN, et al. High-efficiency freezing-induced loading of inorganic nanoparticles and proteins into micron- and submicron-sized porous particles. *Sci Rep*. 2018;8(1), 17763.
31. Novoselova MV, Loh HM, Trushina DB, et al. Biodegradable polymeric multilayer capsules for therapy of lung cancer. *ACS Appl Mater Interfaces*. 2020;12(5):5610–5623.
32. Aherne SA, O'Brien NM. Modulation of cytokine production by plant sterols in stimulated human Jurkat T cells. *Mol Nutr Food Res*. 2008;52(6):664–673.
33. Sanz-Ortega L, Rojas JM, Marcos A, Portilla Y, Stein JV, Barber DF. T cells loaded with magnetic nanoparticles are retained in peripheral lymph nodes by the application of a magnetic field. *J Nanobiotechnol*. 2019;17(1):1–20.
34. Lankoff A, Arabski M, Wegierek-Ciuk A, et al. Effect of surface modification of silica nanoparticles on toxicity and cellular uptake by human peripheral blood lymphocytes in vitro. *Nanotoxicology*. 2012;7(3):235–250.
35. Malysheva A, Ivask A, Doolette CL, Voelcker NH, Lombi E. Cellular binding, uptake and biotransformation of silver nanoparticles in human T lymphocytes. *Nat Nanotechnol*. 2021;16(8):926–932.
36. Vidiasheva IV, Abalymov AA, Kurochkin MA, et al. Transfer of cells with uptaken nanocomposite, magnetite-nanoparticle functionalized capsules with electromagnetic tweezers. *Biomater Sci*. 2018;6(8):2219–2229.
37. Anisimov RA, Gorin DA, Abalymov AA. 3D cell spheroids as a tool for evaluating the effectiveness of carbon nanotubes as a drug delivery and photothermal therapy agents. *C J Carbon Res*. 2022;8(4):56.
38. German SV, Abalymov AA, Kurochkin MA, Kan Y, Gorin DA, Novoselova MV. Plug-and-play lymph node-on-chip: secondary tumor modeling by the combination of cell spheroid, collagen sponge and T-cells. *Int J Mol Sci*. 2023;24(4):3183.
39. Yallapu MM, Chauhan N, Othman SF, et al. Implications of protein corona on physico-chemical and biological properties of magnetic nanoparticles. *Biomaterials*. 2015;46:1–12.
40. Banerjee A, Qi J, Gogoi R, Wong J, Mitragotri S. Role of nanoparticle size, shape and surface chemistry in oral drug delivery. *J Control Release*. 2016;238:176–185.
41. Li F, Ouyang J, Chen Z, Zhou Z, Milon Essola J, Ali B, Wu X, Zhu M, Guo W, Liang XJ. Nanomedicine for T-Cell Mediated Immunotherapy. *Adv Mater*.. 2023, e2301770 https://doi.org/10.1002/adma.202301770.

42. Silva DF, Melo ALP, Uchôa AFC, et al. Biomedical approach of nanotechnology and biological risks: a mini-review. *Int J Mol Sci*. 2023;24(23), 16719.
43. Hillaireau H, Couvreur P. Nanocarriers' entry into the cell: relevance to drug delivery. *Cell Mol Life Sci*. 2009;66(17):2873–2896.
44. Trevaskis NL, Charman WN, Porter CJH. Targeted drug delivery to lymphocytes: a route to site-specific immunomodulation? *Mol Pharm*. 2010;7(6):2297–2309.
45. Tiwari P, Yadav K, Shukla RP, et al. Surface modification strategies in translocating nano-vesicles across different barriers and the role of bio-vesicles in improving anticancer therapy. *J Control Release*. 2023;363:290–348.
46. Gao C, Wang Y, Ye Z, Lin Z, Ma X, He Q. Biomedical micro-/nanomotors: from overcoming biological barriers to in vivo imaging. *Adv Mater*. 2021;33(6).
47. Choi J, Hwang J, Kim J, young, Choi H.. Recent progress in magnetically actuated microrobots for targeted delivery of therapeutic agents. *Adv Healthc Mater*. 2021;10(6).
48. Hua S, de Matos MBC, Metselaar JM, Storm G. Current trends and challenges in the clinical translation of nanoparticulate nanomedicines: pathways for translational development and commercialization. *Front Pharmacol*. 2018;9(JUL).
49. Toy R, Peiris PM, Ghaghada KB, Karathanasis E. Shaping cancer nanomedicine: the effect of particle shape on the in vivo journey of nanoparticles. *Nanomedicine*. 2014;9(1):121–134.